Arab J. Nucl. Sci. Appl., Vol. 58, 2, 53-61 (2025)

ISSN 1110-0451

Arab Journal of Nuclear Sciences and Applications

Web site: ajnsa.journals.ekb.eg

(E S N S A)

Tetragonal Stability in Ceria Zirconia Ceramics Ce-TZP

Kolthoum I. Othman[1]*, Mostafa M. El-Sayed Ali[1], Samia I. El-Houte[1] and Omyma H. Ibrahim[1]

[1] *Metallurgy Department, NRC Nuclear Research Centre, Egyptian Atomic Energy Authority, P.O. Box 137 59, Cairo, Egypt.*

ARTICLE INFO

Article history:

Received: 27th Jan. 2025

Accepted: 26th Feb. 2025

Available online: 15th Mar. 2025

Keywords:

Ce-TZP ceramics;

Coprecipitation;

Tetragonal phase stability;

Toughening mechanisms;

Domain reorientation (switching).

ABSTRACT

Ceria-doped tetragonal zirconia polycrystals (Ce-TZP) exhibit exceptional physical and mechanical properties, making them promising for various applications. This research introduces a novel methodology using XRD analysis on the cut and fracture surfaces of Ce-TZP ceramics, to gain deeper insights into the toughening mechanisms. The sintered ceramic samples have been prepared from powders synthesized via the wet chemical coprecipitation technique with varying ceria content (12-18 mol %). The influence of ceria contents on the tetragonal phase stability of zirconia was investigated as well. X-ray diffraction (XRD), scanning electron microscopy (SEM) and Vickers indentation techniques were used to evaluate the tetragonal phase stability, microstructure, fracture toughness and hardness of the sintered samples, respectively. The results indicated that a stable tetragonal phase predominates at ceria content from 12-18 mol %, whereas below 12 mol %, the tetragonal phase undergoes transformation to the monoclinic phase upon cooling from the sintering temperature. Dense ceramics with high strength and fracture toughness were achieved for sintered zirconia containing 12-18 mol % ceria, with strengths ranging from 430 up to 560 MPa depending on ceria contents. Samples containing 12 mol % ceria, sintered at 1500 °C, exhibited a high toughness (K_{IC}) of 22 MPa$\sqrt{m}$. XRD analysis on cut samples' surfaces, which represents the novelty of the present study, elucidates stress-induced transformation and/or domain reorientation as key toughening mechanisms in Ce-TZP zirconia ceramics.

1. INTRODUCTION

Advanced ceramics, commonly known as engineering or high-performance ceramics, play an integral role across a spectrum of technological sectors, including electronics, telecommunications, automotive, aerospace, industrial machinery, and healthcare. These ceramics exhibit extraordinary properties such as high strength, hardness, elastic modulus, temperature resistance, wear resistance and thermal shock resistance [1, 2].

Among advanced ceramics, Zirconia toughened ceramics, particularly tetragonal zirconia polycrystal ceramics (TZP), achieved through the doping of zirconium oxide with either yttria (Y-TZP) or ceria (Ce-TZP), occupy a prominent position owing to their remarkable strength and toughness, as well as their shape-memory like-behavior [3-5], and transformation plasticity [6]. Ce-TZP, renowned for its chemical stability and catalytic activity for gas purification [7] offers distinct advantages. Furthermore, Ce-TZP ceramic materials can be fabricated with a high degree of metastability [8], and demonstrate superior stability compared to Y-TZP under conditions of low temperature aging [9-11], and in moist environments [2, 10]. However, challenges arise at relatively high temperatures (around 1200 °C), where Ce-TZP may undergo reduction to $Zr_2Ce_2O_7$ resulting in the appearance of a separate phase in a hydrogen-reducing atmosphere [12]. Ce-TZP consistently maintains a singular tetragonal phase within a wide composition range of 12-20 mol % CeO_2, providing ample scope for further exploration [1, 2]. In contrast, the tetragonal phase in Y-TZP is limited to a narrower composition range of 2-3 mol % Y_2O_3 [8]. The physical and mechanical properties of Ce-TZP ceramics, like any ceramic material, are heavily influenced by factors such as; composition, grain size [13-15], impurity content in starting materials [1,16,

Corresponding author: kolthoum.o@yahoo.com

DOI: 10.21608/ajnsa.2025.355746.1875

17], preparation method [13, 15, 18, 19], heterogeneity, and testing methods [20]. Variations in any of these factors, which have been the subject of numerous investigations, could potentially lead to discrepancies in published results.

This study aims primarily to determine the operational toughening mechanisms in Ce-TZP ceramics with different ceria contents employing *a novel technique* utilizing XRD analysis on samples' cut surfaces. Additionally, the study aims to comprehensively investigate the impact of composition on the physical and mechanical properties of sintered Ce-TZP ceramics. To achieve this, various compositions of Ce-TZP powders were prepared using the coprecipitation technique.

2. MATERIALS AND METHODS

Zirconium oxychloride (purchased from BDH chemicals) and Cerous nitrate (obtained from Rare Earth Corporation), served as the starting materials for producing zirconia powders with varying ceria contents, having the chemical formula $Zr_{(1-x)}\ Ce_xO_2$, where x equals 5, 10, 12, 14, 18 mol % of CeO_2. These compositions were denoted as: 5Ce-TZP, 10Ce-TZP, 12Ce-TZP, 14Ce-TZP and 18Ce-TZP, respectively. For each composition, a solution containing 0.2 mole per liter of the calculated proportions of each salt was prepared. Subsequently, an ammonia solution was slowly added to the vigorously stirred mixture, maintaining a pH at 9 during precipitation. The coprecipitation process can be broken down into the following reactions: mixed salt solutions *hydrolysis*, *precipitation* (washing, filtration), and *calcination*.

Hydrolysis:

$(1\text{-}x)\ ZrOCl_2.8H_2O + xCe(NO_3)_3.6H_2O \rightarrow Zr_{1-x}Ce_xO^{2+} + 2(1-x)Cl^- + 3x(NO_3)^- + (8-2x)H_2O$

Precipitation at pH 9:

$(1\text{-}x)ZrOCl_2.8H_2O+xCe(NO_3)_3.6H_2O+2NH_4OH\rightarrow Zr_{1-x}Ce_xO(OH)_2+2(1-x)NH_4Cl+3xNH_4NO_3+(8-2x)H_2O$

The resulting precipitated gel ($Zr_{1-x}Ce_xO(OH)_2$) was then filtered and washed multiple times with distilled water until complete removal of ammonium salts was attained. Following this, the gel was washed with ethyl alcohol and dried at room temperature. Thermal analysis was conducted on the dried gel using a differential thermal analyzer (DTA-50; Shimadzu) and thermogravimetric analyzer (TGA-50; Shimadzu). Based on the thermal analysis results, the dried gel underwent calcination at 600 °C for 3 hours:

$Zr_{1-x}Ce_xO(OH)_2 \rightarrow Zr_{1-x}Ce_xO_2 + 2H_2O$

The resulting calcined powder was subsequently subjected to ball milling and sieving. Rectangular samples were prepared from the different calcined powders using a rectangular steel die with dimensions 35 x 6 mm^2. These samples were pressed at a pressure of 100 MPa, using a compact-type hydraulic press. The geometrically determined average green density was approximately 40 % of the theoretical density (TD). The samples underwent pressureless sintering in air at various temperatures ranging from 1400-1600 °C for one hour. Sintered densities were determined using Archimedes' method. Microstructural features were examined using SEM (Zeiss-Evo10). Prior to SEM examinations, the samples were ground and polished using an Abramine automatic grinding and polishing machine (Struers), followed by thermal etching at 1350 °C for 30 minutes. The average grain size of the sintered samples was computed from SEM micrographs using the linear intercept method [21]. Phase analyses and determination of monoclinic content on the samples' surfaces (as sintered, ground, and cut surfaces) were conducted using X-Ray diffraction (XRD-3A machine with Cu-Ni filter, from Shimadzu). The weight fraction (X_m) and the volume fraction (V_m) of the monoclinic phase were calculated, using Toraya's formula [22], from the integrated peak areas of the lines $[111]_t$, $[111]_m$ and $[\bar{1}11]_m$ of the sintered samples.

$$X_m = \frac{I_m[111]+I_m[\bar{1}11]}{I_m[111]+I_m[\bar{1}11]+I_t[111]} \quad \textbf{(1)}$$

$$V_m = \frac{\mathcal{P}X_m}{1+[\mathcal{P}-1]X_m} \quad \textbf{(2)}$$

Where: $\mathbf{I_m}$ is the intensity of the monoclinic peak, $\mathbf{I_t}$ is the intensity of the tetragonal peak, and $\mathcal{P}$ is a constant equal to 1.333.

Vickers hardness HV in gigapascals (GPa) and fracture toughness stress intensity factor K_{IC} in megapascals square root meter (MPa√m) were calculated from the dimensions of the indentation diagonals and the crack lengths resulting from a Vickers indentation performed on each sample surface, using Zwick Hardness Tester. Measurements of the indentation diagonals and crack lengths were taken at a load of 100 Newton (N) and a 10 seconds dwell time, using an optical microscope equipped with Nomarski interference contrast (EHz-Olympus). For each sample, an average of six indentations measurements was taken. Hardness (HV) and Fracture toughness (K_{IC}) were calculated using the following equations:

$HV = 1.854\ P/d^2$ (3)

$K_{IC} = 0.0725\ Pc^{-3/2}$ (4) Half penny median crack [23]

$K_{IC} = 0.028(HV)^{1/2}.(P/T)^{1/2}$ (5) Palmqvist crack [23]

Where:

P is the load, in Newton.

d is the mean indentation diagonal, in meters (in Equation-3).

c is the crack length from the centre of the indentation to the crack tip (in Equation-4).

T is the total crack length (in Equation-5).

Fracture strength was determined using a four-point bending test conducted on a universal testing machine (LLOYED LR-10 kN). The test employed loading and supporting spans of 10/20 and a crosshead speed of 0.22 mm/min. The average of strength values of four samples for each composition tested was recorded.

3. RESULTS AND DISCUSSION

3.1 Thermal analysis

Figure 1 depicts the results of the differential thermal analysis (DTA) and thermogravimetric analysis (TGA) conducted on the 12Ce-TZP dried gel. The DTA curve exhibits a broad endothermic peak at 119°C, attributed to the removal of adsorbed water and thermal decomposition of zirconium hydroxide into zirconium oxide. Additionally, a sharp exothermic peak at 448 °C corresponds to the crystallization of the amorphous phase of 12Ce-TZP. The TGA curve illustrates significant weight loss occurring between room temperature and 500 °C, indicative of the removal of adsorbed water and the thermal decomposition of zirconium hydroxide. Similar behaviors were observed for the 14Ce-TZP and 18Ce-TZP ceramics. Based on these findings, a calcination temperature of 600 °C was determined to be optimal for producing finely crystallized powders suitable for cold pressing and subsequent sintering after grinding and sieving.

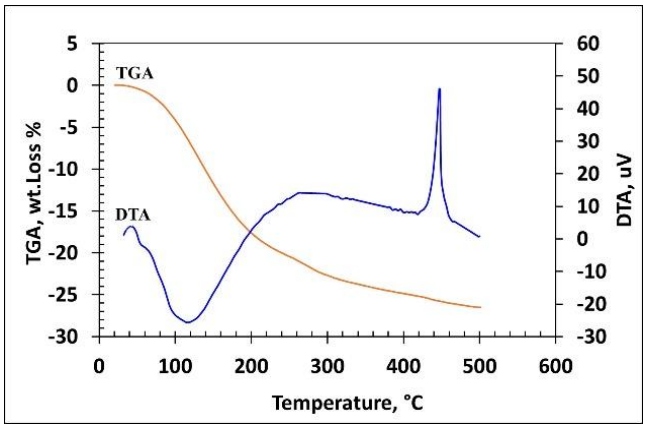

Fig. (1:) Differential thermal analysis (DTA) and Thermogravimetric analysis (TGA) of the 12Ce-TZP dried gel

3.1.2. Density

The sintered samples of Ce-TZP with ceria contents ranging from 12 to 18 mol % exhibited exceptional sintering characteristics. When sintered at 1400 ºC, the samples achieved densities of approximately 97% of theoretical density (TD), while those sintered at both 1500 and 1600 °C reached densities of around 99 % TD. These results align well with findings reported in prior studies [13, 18]. In contrast, a separate study [17] documented low sintered density in a zirconia ceramic containing 17.5 mol % ceria, which was prepared via sol-gel method and sintered at 1600 °C. This discrepancy may be attributed to differences in the specific preparation technique employed in the latter. Similarly, another investigation[19], reported inadequate densification in ceria-zirconia ceramics prepared under industrial condition and sintered at 1710 °C.

Notably, the sintered samples of 5Ce-TZP exhibited cracks induced by the tetragonal to monoclinic (t→m) phase transformation during cooling from the sintering temperature, resulting in very weak mechanical strength. The sintered samples containing 10 mol % ceria (10Ce-TZP) displayed sound surfaces without visible cracks, but with a relatively low density of about 87 % TD and very low strength, indicating an unstable high-temperature tetragonal phase that transformed to a monoclinic phase during cooling from the sintering temperature. Consequently, both the 5Ce-TZP and 10Ce-TZP materials were excluded from further investigation. Previous research [24] suggests that 14 mol % ceria is the minimum amount required for complete stabilization of the tetragonal phase in sintered zirconia ceramics at room temperature.

3.1.3. X-ray diffraction of Ce-TZP sintered ceramics

The X-ray diffraction (XRD) patterns, Fig. 2(a-c), obtained from the surfaces of 12Ce-TZP, 14Ce-TZP, 18Ce-TZP samples sintered at 1500 °C/1 hour, revealed a single tetragonal phase retained at room temperature after cooling from the sintering temperature. This indicates a high degree of stability within the composition range of 12 -18 mol % ceria. The XRD pattern of the as sintered sample containing 12 mol % Ceria is consistent with published data for Ce-TZP ceramics [1, 7, 13, 15], highlighting the prevalence of the tetragonal phase. In contrast, monoclinic phases existed in sintered ceramics containing less than 12 mol % Ceria.

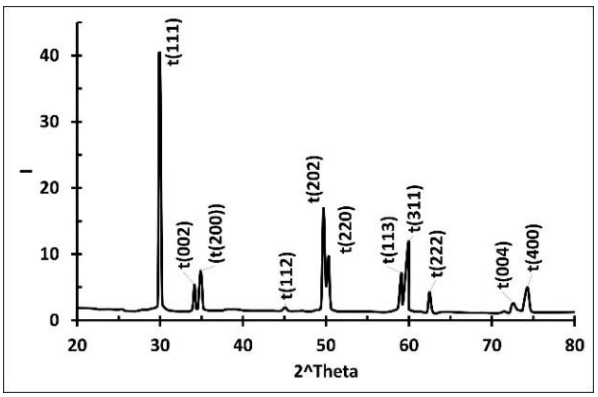

(a)

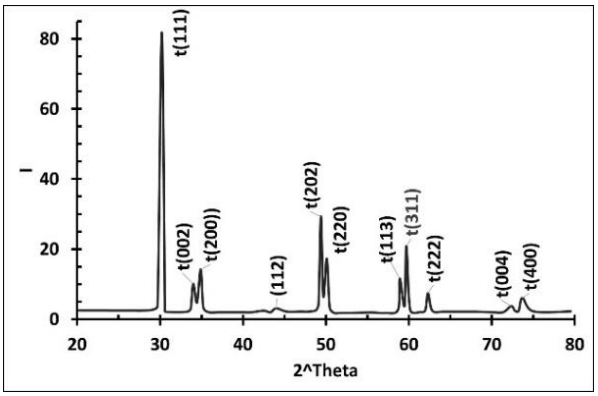

(b)

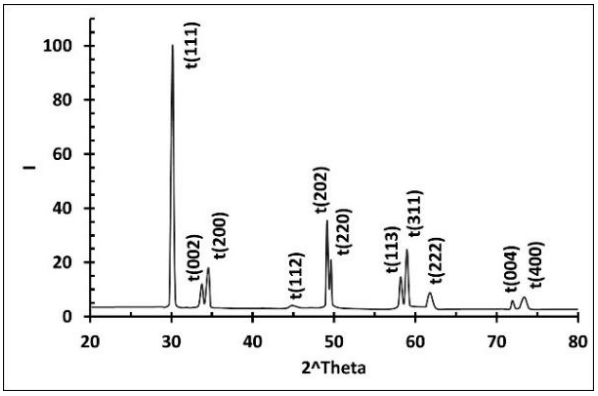

(c)

Fig. (2:) XRD patterns made on the as sintered surfaces of: a) 12Ce-TZP, b) 14Ce-TZP, and c) 18Ce-TZP.

3.2 Microstructure

SEM images of thermally etched surfaces of samples sintered at 1500 °C for 1 hour, containing 12, 14, and 18 mol % Ceria, are presented in Fig. 3(a-c). These microstructures exhibited dense polygonal grain matrices with corresponding grain sizes of 2.3, 1.67 and 1.02 μm, respectively. Notably, the 18Ce-TZP samples displayed relatively smaller grain sizes compared to the other compositions. The average grain size of 2.3 μm observed for 12Ce-TZP was consistent with findings reported in previous studies [13, 25, 26], conducted on similar materials sintered at comparable temperatures.

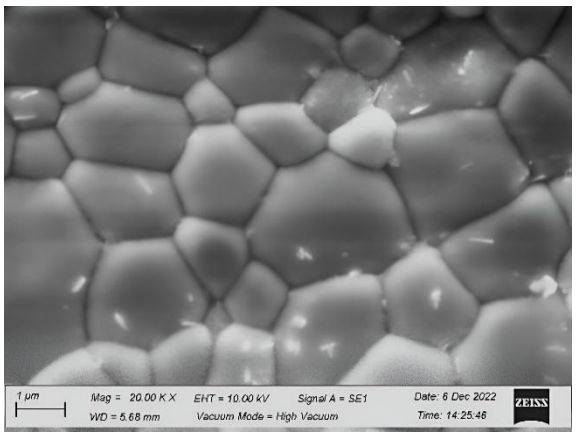

(a)

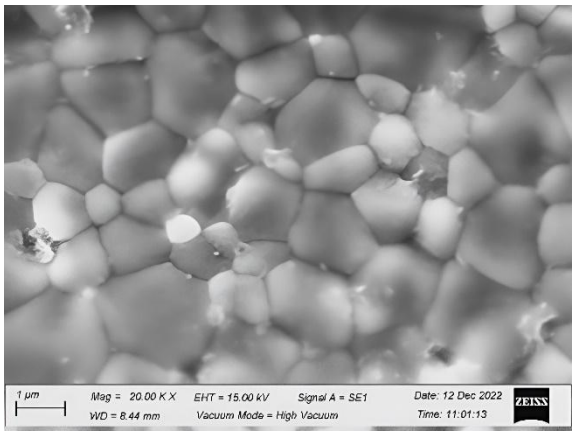

(b)

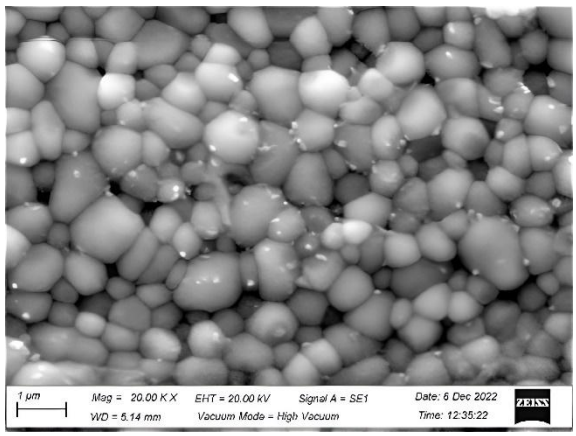

(c)

Fig. (3): SEM micrographs of the thermally etched sintered surfaces of: a) 12Ce-TZP, b) 14Ce-TZP, and c) 18Ce-TZP.

3.3 Mechanical properties

Figure 4 illustrates the variation of the bend strength (MPa), Vickers hardness HV (GPa) and fracture toughness K_{IC} (MPa√m) with ceria content for samples sintered in air at 1500 °C for one hour. It is evident from the figure that the 14Ce-TZP material exhibited the maximum bend strength of 560 MPa, while the maximum fracture toughness K_{IC} of 22 MPa√m was obtained for the

12Ce-TZP. The latter is consistent with published data on fracture toughness measured using Single Edge Notched Beam (SENB) tests of Ce- TZP ceramics containing ceria in the range between 6-16 mol %, which also showed a maximum of K_{IC} value for the material containing 12 mol% ceria [15]. Additionally, the fracture toughness (K_{IC}) was observed to decrease with increasing ceria content, while Vickers hardness demonstrated an increase. These trends align with published findings on Ce-TZP ceramics [1, 12, 15].

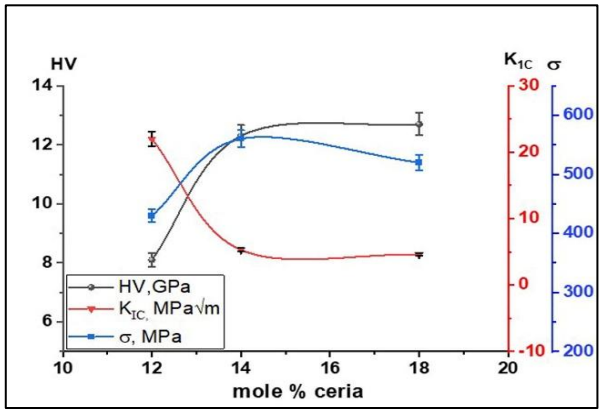

Fig. (4): Vickers hardness, fracture toughness and bend strength as functions of ceria content in Ce-TZP ceramics.

The composition with 12 mol % ceria has been noted to exhibit an increase in fracture toughness with rising sintering temperatures, while Vickers hardness tends to decrease [18]. It is essential to consider that values of fracture toughness, hardness and bend strength are generally influenced by factors such as grain size, sample surface characteristics, and the testing method employed.

Although indentation fracture, which is a non-destructive and easily conducted test, may yield relatively overestimated values of toughness (K_{IC}) compared to other methods for measuring ceramic toughness, it has been utilized in this study solely for the purpose of comparison between the Ce-TZP ceramics with varying ceria contents. Methods like Single Edge Notched Beam (SENB), Single Edge V-notched Beam (SEVNB), Double Cantilever Beam (DCB), and Indentation Strength in Bending (ISB), while reliable, are all destructive techniques.

Figure 5 illustrates the XRD pattern of the fracture surface of the 12Ce-TZP sample alongside those of samples containing 14 and 18 mol % ceria. On the fracture surface of the 12Ce-TZP sample, a considerable amount of monoclinic phase was observed (Fig.5-a), indicating a high-volume percentage (about 80%) resulting from stress-induced transformation of the metastable tetragonal phase. This finding aligns with previously reported data indicating 81 vol % monoclinic phase measured around Vickers indentation, for zirconia ceramic containing 12mol % ceria [25]. In contrast, XRD analysis of the fracture surfaces of the 14Ce-TZP and 18Ce-TZP samples (Fig.5 b, 5-c) revealed only a stable non-transformable tetragonal phase. These results could also be related to grain size, with tetragonal phase stability increasing as grain size decreases and decreasing with a reduction in stabilizer content, consistent with previous investigations on Ce-TZP ceramics [1, 7, 13]. Santos et al., [14] reported that, the higher ceria content in Ce-TZP causes difference in shear stress and alteration in energy necessary for t→m transformation.

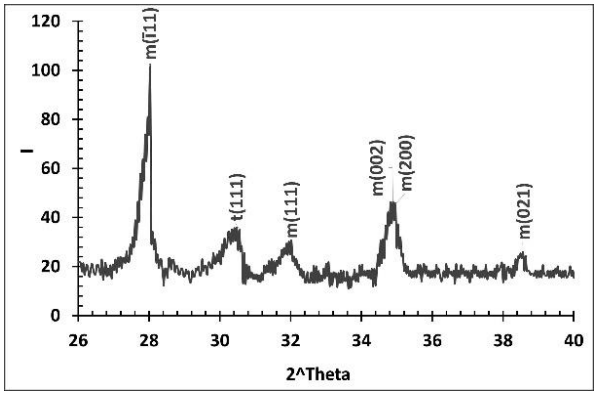

(a)

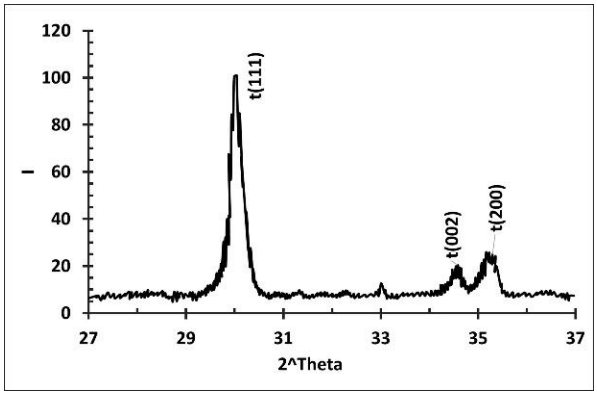

(b)

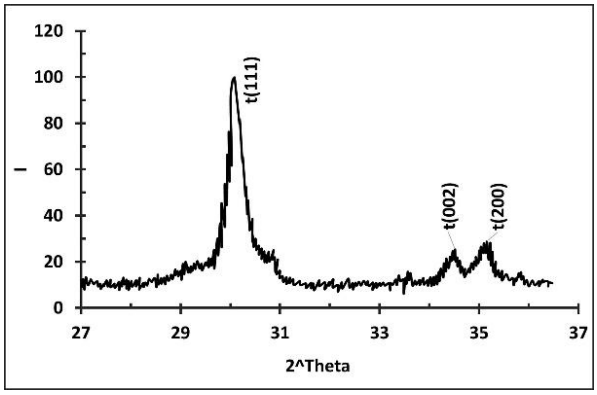

(c)

Fig. (5): XRD patterns of the fracture surfaces of: a)12Ce-TZP, b)14Ce-TZP, and c)18Ce-TZP.

3.3.1 Indentation fracture

Optical micrographs of Vickers indentations on the polished surfaces of 12Ce-TZP and 18Ce-TZP sintered samples (Figures 6 & 7) displayed distinct fracture patterns. The 12Ce-TZP sample exhibited a rosette-like shape obtained using Nomarski interference contrast technique [20, 27], indicative of shear band formation due to significant tetragonal to monoclinic phase transformation which contributes to high fracture toughness. These shear bands result from stress relaxation network of nano-cracks or grain-boundary microcracking associated with transformation plasticity [28]. This explains the non-linear stress-strain behavior observed in the zirconia ceramic containing 12 mol % ceria [9]. These shear bands are designated as transformation bands [29] or deformation bands [14]. In contrast, the 14Ce-TZP and 18Ce-TZP samples showed lateral cracks characteristic of brittle indentation fracture in a Palmqvist crack system.

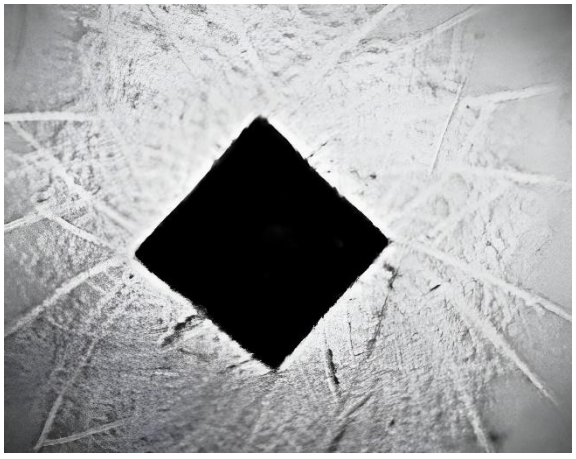

Fig. (6): Optical micrograph of Vickers indentation on the polished surface of 12Ce-TZP sintered sample.

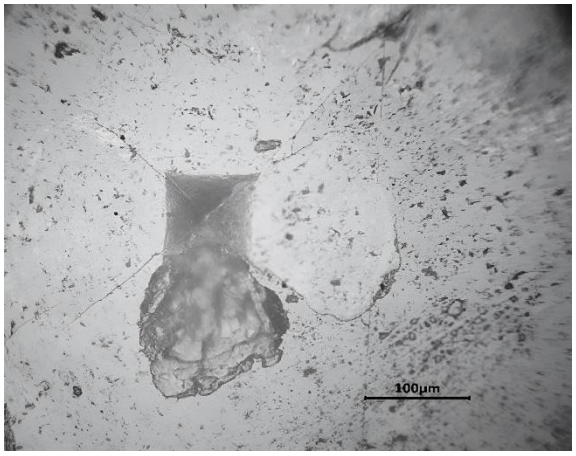

Fig. (7): Optical micrograph of Vickers indentation on the polished surface of 18Ce-TZP sintered sample.

3.3.2 Toughening mechanisms

Regarding toughening mechanisms, XRD patterns performed on the cut surfaces of 12Ce-TZP and 18Ce-TZP samples (Fig. 8-a, 8-b) shed light on the mechanisms acting in each composition. The 12Ce-TZP pattern exhibited appreciable monoclinic phase resulting from stress-induced transformation of the metastable tetragonal phase, alongside the reversal of tetragonal peak intensities of the (002) and (200) lines, which suggests potential simultaneous occurrence of tetragonal to monoclinic phase transformation or transformation toughening and domain switching. This implies that both mechanisms contribute to the high toughness of 12Ce-TZP material [25]. Meanwhile, the X-ray diffraction (XRD) patterns made on both the cut and ground surfaces of samples with higher ceria content (18Ce-TZP) (Fig. 8-b, 8-c) showed no tetragonal to monoclinic transformation, consistent with previous studies [7, 30]. However, there was only a reversal of the intensities of the tetragonal peaks (002) and (200), aligning with prior research [31]. This behavior, also observed in shear-stressed sintered samples of 14Ce-TZP [15], suggests the alternative toughening mechanism called ferro-elastic domain reorientation or switching [26, 32]. The mechanism of transformation toughening in 12Ce-TZP can be elucidated as follows: When the stress around the crack tip reaches a critical point, a phase transformation from tetragonal to monoclinic occurs. This transformed phase, constrained by the surrounding untransformed tetragonal phase, generates a compressive stress in the process zone. This stress effectively opposes crack propagation, thereby increasing the material's toughness.

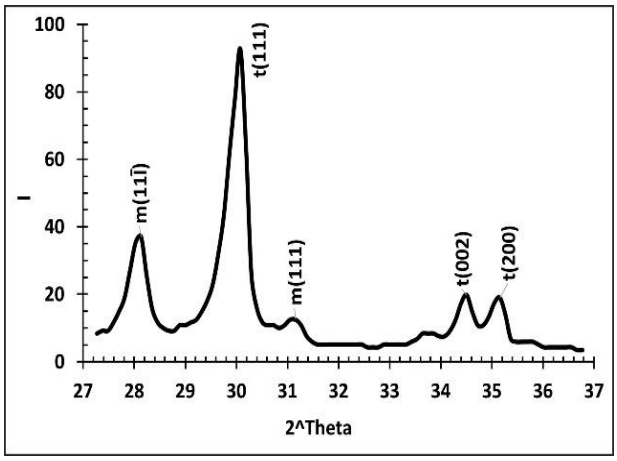

(a)

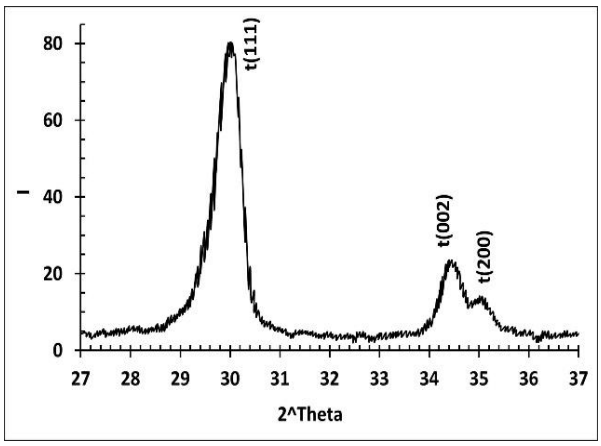

(b)

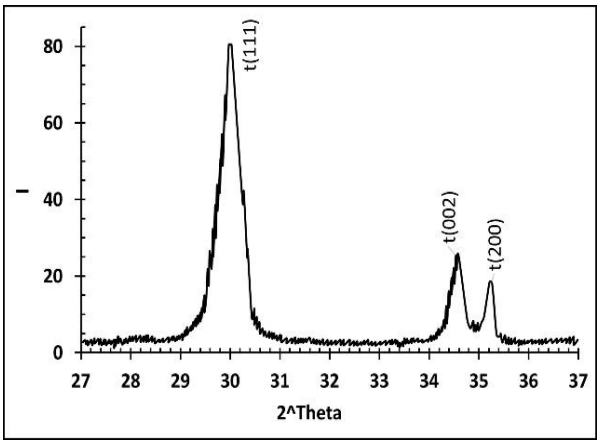

(c)

Fig. (8): XRD patterns of: a) Cut surface of 12Ce-TZP, b) Cut surface of 18Ce-TZP and c) Ground surface of 18Ce-TZP.

Ce-TZP containing ceria from 14 mol % and higher exhibit ferroelastic materials' behavior. The toughness enhancement attributed to domain switching ranges from 5-7 MPa√m for certain compositions of tetravalent oversize ceria-doped zirconia [8].

It's important to distinguish between transformation toughening and domain switching. While both are stress-induced responses, they operate differently. Transformation toughening involves a significant phase change from metastable tetragonal to monoclinic phase, while domain switching entails reorientation of phases within the process zone, absorbing and dissipating crack energy to impede crack propagation and enhance fracture resistance. Ferroelastic reorientation involves transitioning between two equilibrium configurations or tetragonal variants. Additionally, the energy required for domain nucleation or conversion in small grains is lower compared to large grains [33]. This discussion underscores the utility of the X-ray diffraction as a valuable tool in investigating toughening mechanisms in tetragonal zirconia ceramics.

CONCLUSIONS

In this study, homogeneous Ce-TZP ceramic materials with varying ceria contents were prepared using the wet chemical coprecipitation technique. The sintered products exhibited favorable physical and mechanical characteristics. The stability of the tetragonal phase in the sintered Ce-TZP ceramics varied based on the ceria content, ranging from unstable to metastable or stable. Notably, the composition containing 12 mol % ceria demonstrated a metastable transformable tetragonal phase, resulting in a high fracture toughness K_{IC} of 22 MPa√m. Conversely, the material containing 18 mol % ceria displayed a stable tetragonal phase but with lower fracture toughness of 4.6 MPa√m. During indentation, the ceramics with 12 mol % ceria exhibited shear bands around the indentation with a half-penny median crack configuration, while those with 18 mol % ceria displayed lateral cracks with Palmqvist crack configuration. XRD analysis conducted on fracture, cut, and ground samples' surfaces represents the novelty of the present study. It proved to be instrumental in identifying the toughening mechanisms. Overall, this comprehensive investigation underscores the pivotal role of ceria content in modulating the tetragonal stability, as well as the physical and mechanical properties of zirconia ceramics. Furthermore, it emphasizes the significance of both tetragonal to monoclinic phase transformation and domain switching as toughening mechanisms in Ce-TZP ceramics. These findings offer valuable insights for the development of advanced ceramics with enhanced performance.

CONFLICT OF INTERESTS

The authors declare that they have no conflict of interest.

ACKNOWLEDGMENTS

Many thanks and heartfelt gratitude to: *Dr. Ahmed Abdel- Salam, Dr. Mohamed Nashaat El-Shazly* and for all laboratory staff in the metallurgy department/Egyptian Atomic Energy Authority, for their great help to complete this work.

REFERENCES

[1] Tsukuma, K., Shimada, M. (1985) Strength, fracture toughness and Vickers hardness of CeO_2-stabilized tetragonal ZrO_2 polycrystals (Ce-TZP), J. Mater. Sci., 20, 1178–1184.
Doi: 10.1007/BF01026311

[2] Hannink, R.H., Kelly, P.M., Muddle, B.C. (2000) Transformation toughening in zirconia-containing ceramics, J. Am. Ceram. Soc., 83 (3), 461–487. Doi:10.1111/j.11512916.2000.tb01221.x

[3] Mamivand, M., Zaeem, M.A., El Kadiri, H. (2014) Shape memory effect and pseudoelasticity behavior in tetragonal zirconia polycrystals: A phase field study, Int. J. Plast., 60, 71–86. http://dx.doi.org/10.1016/j.ijplas.2014.03.018

[4] Wang, X., Ludwig, A. (2020) Recent developments in small-scale shape memory oxides., Shap. Mem. Superelasticity, 6, 287–300. https://doi.org/10.1007/s40830-020-00299-7

[5] Zeng, X. (2017) Development and characterization of shape memory ceramics at micro/nanoscale., Master's thesis, Nanyang Technological University, (NTU). https://doi.org/10.32657/10356/69895

[6] Tsai, J.F., Chon, U., Ramachandran, N., Shetty, D.K. (1992) Transformation plasticity and toughening in CeO_2-partially-stabilized zirconia–alumina (Ce-TZP/Al_2O_3) composites doped with MnO, J. Am. Ceram. Soc., 75 (5), 1229–1238. https://www.academia.edu/en/31532913

[7] Liu, X.-M. (2021) The influence of cerium oxide content on the crack growth in zirconia ceramic materials for engineering applications, Results Mater., 10, 100196. https://doi.org/10.1016/j.rinma.2021.100196

[8] Chevalier, J., Gremillard, L. (2009) The tetragonal-monoclinic transformation in zirconia: lessons learned and future trends. J. Am. Ceram. Soc., 92 (9), 1901–1920. https://doi.org/10.1111/j.1551-2916.2009.03278.x

[9] Lughi, V., Sergo, V. (2010) Low temperature degradation-aging-of zirconia: A critical review of the relevant aspects in dentistry, J. Dent. Mater., 26 (8), 807-820. https://doi.org/10.1016/j.dental.2010.04.006

[10] Chevalier, J., Liens, A., Reveron, H., Zhang, F., Reynaud, P., Douillard, T., Preiss, L., Sergo, V., Lughi, V., Swain, M., Courtois, N. (2020) Forty years after the promise of «ceramic steel?»: Zirconia-based composites with a metal-like mechanical behavior, J. Am. Ceram. Soc., 103 (3), 1482–1513. https://doi.org/10.1111/jace.16903

[11] Reveron, H., Liens, A., Chevalier, J., Fornabaio, M., Palmero, P., Montanaro, L., Fürderer, T., Schomer, S., Adolfsson, E., Courtois, N. (2019) New “ductile” zirconia-based ceramics for the development of dental implants, Comput Methods Biomech Biomed. Engin., 22 (sup1), S68–S70. https://doi.org/10.1080/10255842.2020.1713482

[12] Zhu, H.Y., Hirata, T., Muramatsu, Y. (1992) Phase separation in 12 mol % ceria-doped zirconia induced by heat treatment in H_2 and Ar, J. Am. Ceram. Soc., 75 (10), 2843–2848. https://doi.org/10.1111/j.1151-2916.1992.tb05514.x

[13] Quinelato, A.L., Longo, E., Perazolli, L.A., Varela, J.A. (2000) Effect of ceria content on the sintering of ZrO_2 based ceramics synthesized from a polymeric precursor, J. Eur. Ceram. Soc., 20 (8), 1077–1084. https://doi.org/10.1016/S09552219(99)00269-1

[14] Dos Santos, C., Coutinho, I.F., Amarante, J.E., Pais Alves, M.F.R., Coutinho, M.M., da Silva, C.R.M. (2021) Mechanical properties of ceramic composites based on ZrO_2 co-stabilized by Y_2O_3–CeO_2 reinforced with Al_2O_3 platelets for dental implants, J. Mech. Behav. Biomed.l Mater., 116, 104372 [1–12]. https://doi.org/10.1016/j.jmbbm.2021.104372

[15] Sharma, S.C., Gokhale, N.M., Dayal, R., Lal, R. (2002) Synthesis, microstructure and mechanical properties of ceria stabilized tetragonal zirconia prepared by spray drying technique, Bull. Mater. Sci., 25 (1), 15–20. https://doi.org/10.1007/BF02704588

[16] Ibrahim, O.H., Othman, K.I., Hassan, A.A., El-Houte, S., Ali, M.E.-S. (2020) Effect of gadolinia addition on the mechanical and physical properties of zirconia/ceria ceramics, SN Appl. Sci., 2 (10), 1755. https://doi.org/10.1007/s42452-020-03578-1

[17] Naga, S.M., Ahmed, M.A., Sayed, A.Z., Farag, R.S., Abdelmegeed, A.F. (2017) Effect of ceria on the properties of ceria stabilized zirconia/ alumina/ ceria (ZTA/Ce) composites, Elixir Appl. Chem., 102, 44354–44358. https://www.researchgate.net/publication/312317033

[18] Ali, M.E.-S., El-Houte, S., Sørensen, O.T. Properties of ceria doped tetragonal zirconia ceramics prepared by coprecipitation technique, 11th Risø International

Symposium on Metallurgy and Materials Science., Riso, Denmark, (1990).

[19] Zhao, L., Yao, S., Du, J., Huang, Q., Sun, H. (2019) Preparation and characterization of ceria partially stabilized zirconia ceramics. 2nd International Conference on Frontiers of Materials Synthesis and Processing, IOP Conf. Series: Materials Science and Engineering 493, 012082. https://doi.org/10.1088/1757-899X/493/1/012082

[20] Touaiher, I., Saâdaoui, M., Chevalier, J., Preiss, L., Reveron, H. (2018) Fracture behavior of Ce-TZP/alumina/aluminate composites with different amounts of transformation toughening. Influence of the testing methods, J. Eur. Ceram. Soc., 38 (4), 1778–1789. http://dx.doi.org/10.1016/j.jeurceramsoc.2017.09.052

[21] Wurst, J., Nelson, J.A. (1972) Linear intercept technique for measuring grain size in two-phase polycrystalline ceramics, J. Am. Ceram. Soc., 55 (2), 109. https://doi.org/10.1111/j.1151-2916.1972.tb11224.x

[22] Toraya, H., Yoshimura, M., Somiya, S. (1984) Calibration curve for quantitative analysis of the monoclinic-tetragonal ZrO_2 system by X-ray diffraction, J. Am. Ceram. Soc., 67 (6), C-119–C-121. https://doi.org/10.1111/j.1151-2916.1984.tb19715.x

[23] Ćorić, D., Ćurković, L., Renjo, M.M. (2017) Statistical analysis of Vickers indentation fracture toughness of Y-TZP ceramics, Trans. FAMENA., 41 (2), 1–16. Doi:10.21278/TOF.41201

[24] A. K. Pandey, K. Biswas. (2011) Influence of sintering parameters on tribological properties of ceria stabilized zirconia bio-ceramics, Ceram. Int., 37 (1), 257–264. https://doi.org/10.1016/j.ceramint.2010.08.041

[25] Zhang, W., Bao, J., Xu, J., Wu, X., Li, D., Song, X., An, S. (2017) Composition dependence of the adjustable microstructure and mechanical properties of ytterbia-ceria-costabilised TZP, J. Alloys Comp., 727, 627–632. http://dx.doi.org/10.1016/j.jallcom.2017.08.176

[26] Chevalier, J., Gremillard, L., Zenati, R., Jorand, Y., Olagnon, C., Fantozzi, G. (2002) Slow crack growth in zirconia ceramics with different microstructures, Fract. Mech., 13, 287–303. https://doi.org/10.1007/978-1-4757-4019-6_23

[27] Heussner, K.-H., Claussen, N. (1989) Yttria-and ceria-stabilized tetragonal zirconia polycrystals (Y-TZP, Ce-TZP) reinforced with Al_2O_3 platelets, J. Eu. Ceram. Soc., 5 (3), 193–200. https://doi.org/10.1016/0955-2219(89)90035-6

[28] Liens, A., Reveron, H., Douillard, T., Blanchard, N., Lughi, V., Sergo, V., Laquai,R., Müller, B. R., Bruno, G., Schomer, S., Fürderer, T., Adolfsson, E., Courtois, N., Swain, M., Chevalier., J. (2020) Phase transformation induces plasticity with negligible damage in ceria-stabilized zirconia-based ceramics, Acta Mater, 183, 261–273. https://doi.org/10.1016/j.actamat.2019.10.046

[29] Liens, A., Swain, M., , Reveron, H., Cavoret, J., Sainsot, P., Courtois, N., Fabrègue, D., Chevalier, J. (2021) Development of transformation bands in ceria-stabilized-zirconia based composites during bending at room temperature, J. Eu. Ceram. Soc., 41 (1), 691–705. https://doi.org/10.1016/j.jeurceramsoc.2020.08.062

[30] Tsukuma, K., (1986) Mechanical properties and thermal stability of CeO/sub2/ containing tetragonal zirconia polycrystals, Am. Ceram. Soc. Bull., 65 (10), 1386–1390.

[31] Wongkamhaeng, K., Dawson,D.V., Holloway, J.A., Denry, I. (2019) Effect of surface modification on in-depth transformations and flexural strength of zirconia ceramics, J. Prosthodont., 28 (1), e364–e375. https://doi.org/10.1111/jopr.12908

[32] Deville, S., El Attaoui, H., Chevalier, J. (2005) Atomic force microscopy of transformation toughening in ceria-stabilized zirconia, J. Eu. Ceram. Soc., 25 (13), 3089–3096. https://doi.org/10.1016/j.jeurceramsoc.2004.07.029

[33] Zeng, Z., Liu, Y., Zhang, Y., Zhou, Z., Liu, X. (2020) Ferroelastic domain switching toughening in Ce–Y–La co-stabilized zirconia ceramics obtained from coated starting powders, J. Alloy. Compd., 820, 153177[1-8] . https://doi.org/10.1016/j.jallcom.2019.153177